Real-Time Demonstration of Augmented-Spectral-Efficiency DMT Transmitter using a Single IFFT

Qibing Wang, Binhuang Song, Bill Corcoran, *Member, IEEE*, Leimeng Zhuang, *Senior Member, IEEE*, and Arthur James Lowery, *Fellow, IEEE*

***Abstract*—Increasing the power and spectral efficiency in intensity modulated direct-detection short-haul fiber-optic links enables higher data rates in power- and bandwidth-limited optical communication systems. Augmented spectral efficiency discrete multi-tone (ASE-DMT) can improve the spectral efficiency of pulse-amplitude-modulated DMT while maintaining its power advantage over DC-biased DMT, whose transmitter requires only one inverse fast Fourier transform (IFFT) with Hermitian symmetric inputs. Although the ASE-DMT transmitter requires multiple IFFTs, we show how these can be mapped onto a single IFFT, by using both the real and imaginary outputs of the IFFT and by extracting some signals from within the IFFT's structure. Using only one IFFT, we firstly demonstrate a real-time PAM4-encoded optical ASE-DMT transmitter with a net data rate of 18.4 Gb/s. When implemented in a FPGA, using a single IFFT saves 30% of logic resources, compared with a four-IFFT ASE-DMT transmitter. Finally, a 1550-nm directly modulated laser is used to evaluate its optical transmission performance with off-line signal processing in the receiver. Without using any optical amplifiers, the ASE-DMT signal can be successfully transmitted over 10-km standard single-mode fiber (SSMF), but fails over 20-km SSMF due to the influence of fiber dispersion and laser chirp.**

***Index Terms*—Discrete multi-tone, real-time systems, hardware efficiency, directly modulated laser.**

I. Introduction

OPTICAL orthogonal frequency division multiplexing (OFDM), has been explored for both long-haul [1], [2] and short-haul [3], [4] optical communications due to its wide adoption in wireless communications. In short-haul transmission, OFDM is often called discrete multi-tone (DMT). The rapid development of bandwidth-hungry applications such as big data and high-definition video streaming demand speed upgrades of short-haul datacenter interconnects. In contrast to long-haul optical communication systems using external modulation and coherent detection, datacenter optical interconnects are very cost- and size-sensitive. Therefore, intensity modulation and direct-detection (IMDD) using directly modulated lasers (DML) is more attractive because it promises low cost and small size.

Four-level pulse amplitude modulation (PAM4) and DMT are the two main candidates for high-speed datacenter interconnects. PAM4 is preferred for links shorter than 10 km, as it does not require high-resolution DACs and ADCs. However, compared with PAM4, DMT can adapt its modulation format of different subcarriers through bit-loading and power-loading to avoid dispersion-induced nulls in the link's baseband frequency response. Therefore, it is more suitable for >10-km links, so has been widely explored using offline [5]-[7] and real-time [8]-[10] digital signal processing (DSP). However, all of these DMT systems require a large DC bias to avoid clipping of negative-going peaks, which translates to wasted optical power. Such schemes are called DC-biased optical OFDM (DCO-OFDM) in this paper. Therefore, the power efficiency of DCO-OFDM needs to be improved by lowering or eliminating the DC bias. The two most well-known techniques are asymmetrically clipped optical OFDM (ACO-OFDM) [11] and pulse-amplitude-modulated optical DMT (PAM-DMT) [12]. For both the ACO-OFDM and PAM-DMT schemes, unipolar outputs are achieved by clipping the negative drive currents to zero. However, these two schemes cannot use the even-valued subcarrier slots (ACO-OFDM) or the in-phase components (PAM-DMT); thus, they sacrifice half of the spectral efficiency. Therefore, compared with DCO-OFDM at the same data rate, they require either higher-order modulation formats, or electrical and optical devices with doubled bandwidths. As a result, DCO-OFDM is preferable for single-laser 100 Gb/s short-haul links [13].

More recently, layered/enhanced ACO-OFDM (L/EACO-OFDM) has been developed to improve the spectral efficiency of ACO-OFDM towards that of DCO-OFDM, by enabling the even-frequency subcarriers to be used [14]-[18]. Similarly, augmented spectral efficiency DMT (ASE-DMT) uses layering applied to PAM-DMT, allowing the unused in-phase components to be modulated in additional layers [19]. As the

This paragraph of the first footnote will contain the date on which you submitted your paper for review. This work is supported under the Australian Research Council's Laureate Fellowship (FL130100041) scheme and CUDOS – ARC Centre of Excellence for Ultrahigh-bandwidth Devices for Optical Systems (CE110001018).

Qibing Wang, Binhuang Song, Bill Corcoran, Leimeng Zhuang and Arthur James Lowery are with the Electro-Photonics Laboratory, Dept. of Electrical and Computer Systems Engineering, Monash University, Clayton, VIC 3800, Australia. (e-mail: qibing.wang@monash.edu; binhuang.song@monash.edu; bill.corcoran@monash.edu;leimeng.zhuang@monash.edu;arthur.lowery@monash.edu).

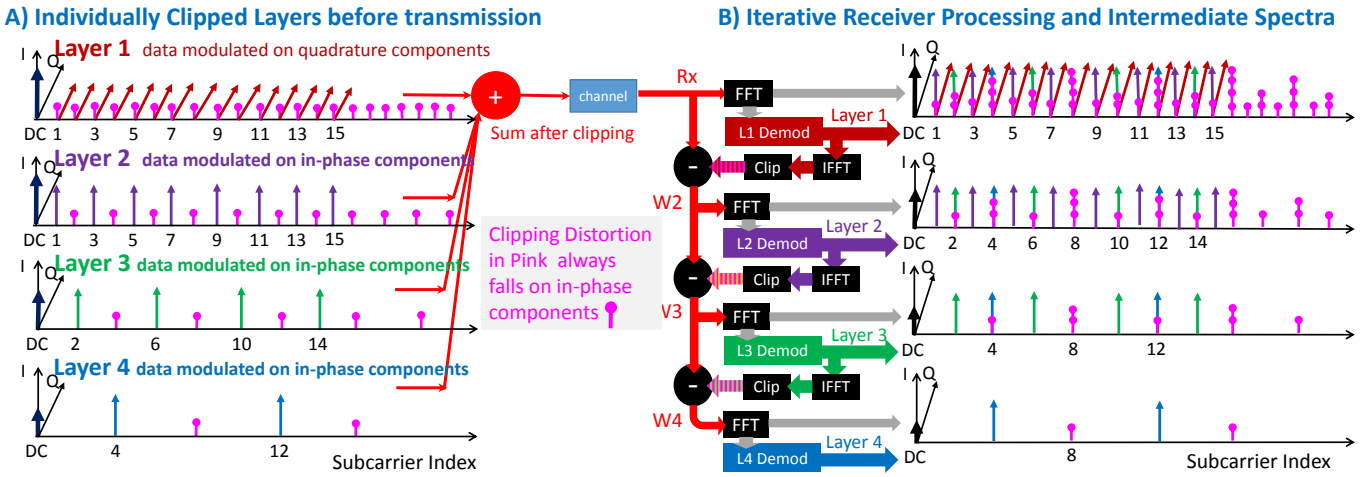

Fig. 1. Data-carrying subcarrier allocation in an ASE-DMT transmitter (left) and iterative decoding (center) and spectra (right).

clipping procedure is also performed in all the layers for both L/EACO-OFDM and ASE-DMT, these two schemes still maintain a power advantage over DCO-OFDM without halving the spectral efficiency. The first hardware-efficient real-time L/EACO-OFDM transmitter has been demonstrated [20]. However, an efficient real-time ASE-DMT transmitter has yet to be experimentally demonstrated.

In this paper, we firstly introduce a novel and efficient method of generating ASE-DMT signals. This paper is an extension of the work presented in ECOC 2017 [21]. In addition to upgrading the modulation format to PAM4, here we also give a more detailed description of the mapping algorithm and transmission performance evaluation over fiber. Through carefully mapping the layers to the inputs of one inverse fast Fourier transform (IFFT) and by extracting the higher layer's waveforms from within the core of one IFFT, separate outputs for each layer can be obtained, to be clipped separately before combination. Using this method, a real-time PAM4-encoded ASE-DMT transmitter is implemented in a Virtex-6 FPGA. Its net output data rate is up to 18.4 Gb/s. A Q-factor of 19.67 dB is obtained for an optical back-to-back experiment. Using a 1550-nm DML, the signal can be successfully transmitted over 10-km standard single-mode fiber (SSMF) with a Q-factor of 18.51 dB.

The paper is organized as follows. In Section II, we will give a brief introduction of ASE-DMT algorithm. In Section III, the method to extract outputs of all the layers in one IFFT module will be discussed, followed by a full implementation of the DSP in a FPGA-based ASE-DMT transmitter. In Section IV, the short-haul transmission link will be briefly described. Then the fiber transmission distance of ASE-DMT signal will be examined using a 1550-nm DML in Section V, before giving a conclusion in Section VI.

II. ASE-DMT Algorithm

In PAM-DMT, if only the quadrature components (imaginary parts) of all the subcarriers are modulated, the clipping distortion falls only on the in-phase components (real parts) of all the subcarriers [12]. As illustrated in Fig. 1(A), to enable these in-phase components to carry data, ASE-DMT adds further layers on-top of these distortion. Four layers are used in this illustration and more layers can be used until the in-phase and quadrature components of all the subcarriers are encoded to give the same spectral efficiency of DCO-OFDM if necessary. The first layer of ASE-DMT, which is the same as PAM-DMT, carries pulse-amplitude-modulated signal on the quadrature components of all the subcarriers. Therefore, its clipping distortion only falls on the in-phase components of all the frequencies [12]. The higher layers, L (2, 3, 4), carry pulse-amplitude-modulated signals on the in-phase components of subcarriers that have frequency indices $(2n+1)\times 2^{(L-2)}$, where n = (0, 1, 2, 3, …). Clipping these produces distortion that also falls on the in-phase components. However, as with L/EACO-OFDM [20], its clipping distortion only falls on the subcarriers that have frequency indices $2n\times 2^{(L-2)}$, where n = (1, 2, 3, …). To build the ASE-DMT signal, each layer generates its own outputs using a separate inverse fast Fourier transform (IFFT); then the negative values of each layer's waveform are clipped to become zero-valued. Finally, a unipolar signal output is obtained by adding all the already-clipped waveforms of the four layers.

From Fig. 1(A), it is clear that the clipping distortion from all the layers only falls on the in-phase components. Therefore, Layer 1 is free of clipping distortion, and so is decoded firstly, using a FFT and a slicer. This recovered data can then be used to regenerate a facsimile of Layer 1's transmitted waveform using an IFFT and a clipper, which is then subtracted from the received waveform, to reveal the in-phase components of higher layers as shown in Fig. 1(B). Now the in-phase components in Layer 2 become free of clipping-distortion, so can be decoded next. The same procedure is repeated layer by layer until the data in all the layers are recovered. A more detail analysis of this iterative receiver can be found in [19].

III. ASE-DMT Transmitter Implementation

A. IFFT Implementation

As one IFFT module is required in every layer in the ASE-DMT transmitter, it will significantly increase the overall

computational complexity because IFFT itself will occupy most of the logic resources of the transmitter's FPGA. Considering only multipliers, Islim *et al*. have estimated that the computational complexity of ASE-DMT transmitter is the same as a quadrature-amplitude-modulated (QAM) DCO-OFDM transmitter for the same spectral efficiency, because only the real-valued or the imaginary-valued frames in the ASE-DMT transmitter need be computed, avoiding a complex IFFT [19]. However, they still required several separate IFFT modules, which had to be optimized individually to reduce the overall computational complexity, making the implementation more complicated. We now experimentally demonstrate that: (a) re-arranging the IFFT's inputs and (b) extracting signals from within the IFFT, reduces the computation for all layers of ASE-DMT to that of one complex IFFT. This algorithm requires only a slight change to a standard IFFT module.

In a standard QAM DCO-OFDM transmitter, one IFFT module is used to generate and superpose all the subcarriers digitally. For a 2*N*-point IFFT, the OFDM time domain signals over one symbol can be written as

$$x(n)=\frac{1}{2N}\sum_{k=0}^{2N-1}X(k)\exp\left(\frac{j2\pi kn}{2N}\right),\ n=0,1,...,2N-1 \quad (1)$$

where $X(k) = D(k) + jE(k)$ (k =0, 1, …, 2N-1) are the QAM-modulated inputs to the IFFT module. Hermitian symmetry ($X(2N\text{-}k) = X^*(k)$, k =1, 2, …, 2N-1) with ($X(0) = X(N) = 0$) is usually imposed on the IFFT inputs. Therefore, Equation (1) can be simplified to

$$x(n)=\frac{2}{2N}\sum_{k=0}^{N-1}\left[D(k)\cos\left(\frac{2\pi kn}{2N}\right)-E(k)\sin\left(\frac{2\pi kn}{2N}\right)\right],\ n=0,1,...,2N-1 \quad (2)$$

From Equation (2), it can be seen that the imaginary values at the IFFT's output are forced to be zero. These real parts are often used to drive optical modulator or laser. Alternatively, IFFT's input pairs with the same imaginary part but the negated real part ($X(2N\text{-}k) = -X^*(k)$, k =1, 2, …, 2N-1. $X(0) = X(N) = 0$), which is named skew-Hermitian symmetry, can be used to force the real parts of the IFFT's output to zero, producing a signal only at its imaginary outputs. This can be concluded from Equation (3), which is written for when $X(k)$ has skew-Hermitian symmetry.

$$x(n)=\frac{2j}{2N}\sum_{k=0}^{N-1}\left[D(k)\sin\left(\frac{2\pi kn}{2N}\right)+E(k)\cos\left(\frac{2\pi kn}{2N}\right)\right],\ n=0,1,...,2N-1 \quad (3)$$

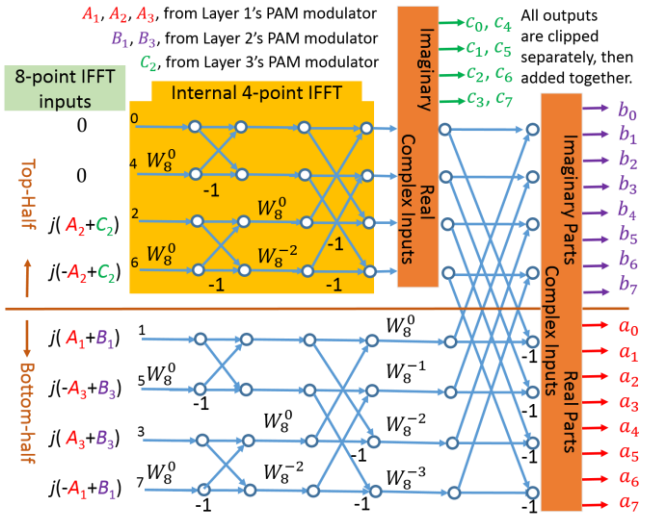

Fig. 2. An 8-point 2-radix decimation-in-time IFFT butterfly flow chart.

Therefore, if we put both the Hermitian symmetric and skew-Hermitian symmetric signals as the IFFT's inputs at the same time, we can obtain corresponding waveforms from the real and imaginary parts of IFFT's outputs. This is based on the idea that one complex-valued FFT can be used to compute two real-valued FFTs [22]. For L/EACO-OFDM, Wang *et al*. have shown that smaller IFFT sizes can be used in the higher layers because the signals in higher layers are periodic [15]. As the ASE-DMT signals also use different layers to remove the clipping distortion, smaller IFFT sizes can also be applied to the hardware implementation of higher layers in the ASE-DMT transmitter. By using both the real and imaginary parts of IFFT and using smaller IFFTs in higher layers, we show that only one IFFT is required to generate the unclipped waveforms of all layers.

Fig. 2 illustrates how a complex 8-point decimation-in-time (DIT) IFFT butterfly can generate separate outputs for three layers simultaneously. The $X(0)$ and $X(4)$ inputs of the 8-point IFFT are zero-valued. Modification (a) Layer 1's PAM modulator outputs (A_1, A_2, A_3) and their Hermitian counterparts ($-A_1$, $-A_2$, $-A_3$) are assigned to the imaginary IFFT inputs; Layer 2's PAM modulator outputs (B_1, B_3) and their skew-Hermitian counterparts (B_1, B_3) are also assigned to the same imaginary IFFT inputs but only in the bottom-half; Layer 3's PAM modulator output (C_2) and its skew-Hermitian

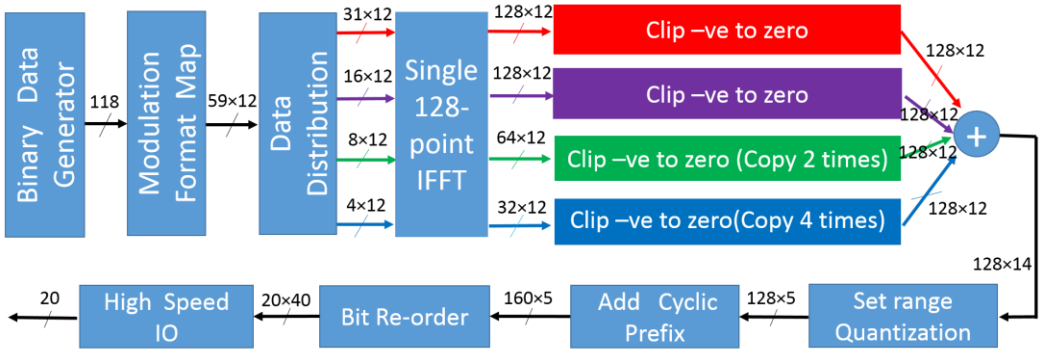

Fig. 3. DSP functions implemented in the FPGA with a single 128-point IFFT. $A \times B$: A' parallel data-streams are transmitted and each has a B-bit resolution.

counterpart (C_2) are added to some of the top-half imaginary IFFT inputs. Although all the PAM4 signals from all layers are input to the imaginary parts of the IFFT, they are steered separately to the real parts (a_n) and imaginary parts (b_n and c_n) of the IFFT's outputs. This is because that the PAM4 signal from the first layer has Hermitian symmetry; whereas the PAM4 signals from the second and third layers have skew-Hermitian symmetry.

However, as the results (b_n and c_n) from Layer 2 and Layer 3 both flow to the imaginary outputs of IFFT, we need to separate them within the IFFT butterfly before their data flows interact. Modification (b) uses the convenient fact that the top/bottom data flows in complex IFFTs are separate except in the final butterfly. Thus, the 4-point sub-IFFT (orange area in Fig. 2) is used for Layer 3, and similarly the bottom-half computations for Layer 2. Our innovation is to extract the output of the sub-IFFT of Layer 3 (c_n) before the final butterfly, so that the outputs of Layer 2 are not polluted by the outputs of Layer 3. This is achieved by separating the real and imaginary parts of the data just after the 4-point sub-IFFT: the imaginary parts become Layer 3's real waveform after the block (c_1, c_2, c_3, c_4) is duplicated. The real parts of the orange area flow into the final butterfly, which calculates the waveforms for Layer 1. Conveniently, Layer 1 (a_n) is contained in the real parts of the IFFT's final outputs and Layer 2 (b_n) is in its imaginary parts. Thus these two waveforms can be separately clipped before summation with Layer 3's clipped waveform. By applying Modification (b) multiple times, ASE-DMT transmitter with more than 3 layers can also be implemented using one IFFT.

B. Transmitter DSP Implementation

From Section 2, we can see that four layers will give the 93.75% (= 1/2 + 1/4 + 1/8 + 1/16) spectral efficiency of DCO-OFDM. By further increasing the number of layers, the ASE-DMT will eventually achieve the same spectral efficiency as DCO-OFDM. However, as the iterative receiver needs to repeat the decoding process for each layer, there is a trade-off between increasing spectral efficiency and reducing computational complexity. Four layers were used in our experimental demonstration.

The Spiral™ FFT/IFFT IP Core Generator [23] was used to generate one fully-streaming 128-point IFFT Verilog code. In this experimental demonstration, we slightly modified the generated Verilog code in order to extract the temporary calculation results within the IFFT module. All the DSP functions were implemented in a Virtex-6 FPGA chip. Fig. 3 shows DSP functions performed in the FPGA. The test data and two training symbols were stored in the FPGA. For each clock cycle, 118 data bits were mapped to 59 PAM4 symbols. The IFFT core used 12-bit resolution, which was carefully selected as a compromise between computational accuracy and hardware resource occupation [20]. Afterwards, these 59 symbols, combined with their Hermitian counterparts, were distributed to the four layers through a data distribution module in the way as illustrated in Fig. 2. Within the IFFT module, the waveforms of each layer were extracted at different IFFT butterfly stages. As the IFFT module was fully pipelined, in order to align the outputs in all the layers, additional registers were added to delay the outputs of higher layers by a certain number of clocks. In each layer, the waveforms were clipped to remove all negative values and then repeated to form 128 12-bit real words before being added together. In order to reduce the required number of adders, the same adding procedure was used as the real-time L/EACO-OFDM transmitter in [20]. The set-range and quantization module transformed the 128 14-bit words into 128 5-bit words, each being a sample of the OFDM waveform within one OFDM symbol. Then a 32-sample cyclic prefix (CP) was pre-pended to every OFDM symbol, producing 160 5-bit words. The DAC required four data streams at one quarter of the sample rate, thus 20 FPGA's LVDS (low voltage differential signaling) channels must be used, each at a rate of 6.25 Gbaud. The DAC multiplexed these 4 channels,

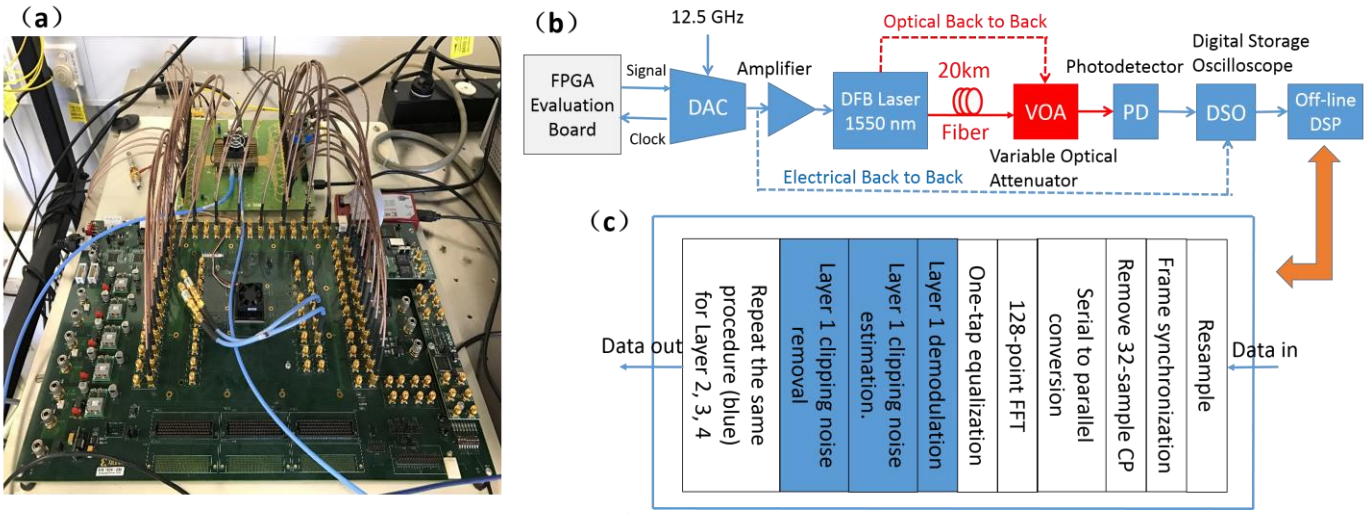

Fig. 4. ASE-DMT optical transmission link setup: (a) Connection setup of FPGA and DAC: the DAC board has a 12.5-GHz clock input and it generates a 156.25-MHz clock fed to FPGA, whose outputs are transmitted to the DAC to generate an analog signal, (b) Setup diagram, (c) Off-line DSP algorithm performed in MATLAB.

then produced a 25 Gsample/s 5-bit resolution analog output.

TABLE I
KEY PARAMETERS IN THE EXPERIMENTAL SETUP

Parameter	Value
Modulation format	PAM4
Oversampling rate	2
Number of layers	4
IFFT size	128-point
IFFT resolution	12 bits
CP length	32 samples
FPGA fabric clock	156.25 MHz
DAC clock	12.5 GHz
DAC output voltage	500 mV
DAC sampling rate	25 GSa/s
DAC resolution	5 bits
Net bit rate	18.4 Gb/s
DFB laser wavelength	1550 nm
DFB laser bias current	36 mA
Amplifier bandwidth	40 GHz
Oscilloscope sampling rate	80 GSa/s
Photodetector bandwidth	16 GHz
Single-mode fiber length	10 km and 20 km

C. Logic Resource Utilization

In the previous sections, we have shown that the ASE-DMT transmitter can be implemented in the FPGA using only one 128-point IFFT. This is called Scheme 1. In order to see its hardware resource utilization advantage, another ASE-DMT transmitter was also implemented in the FPGA using four IFFT modules, which is called Scheme 2. In Layer 1, a 128-point IFFT was used. In Layers 2, 3 and 4, 128-point, 64-point and 32-point IFFTs were used. We optimized the IFFT Verilog code of Layers 2, 3 and 4 to only calculate the bottom-half of the butterfly chart, as these three layers had regular zero-valued IFFT's inputs [20]. The other DSP functions were all the same for these two schemes, as shown in Fig. 3.

Of the available resources on the Vertix-6 FPGA (XC6VLX240T), it was reported by the Xilinx Integrated Synthesis Environment (ISE) that the Scheme 1 used 13% of the slice registers (40944), 21% of the slice LUTs (32682) and 134% of the DSP48E1s (1036) and the Scheme 2 used 18% of the slice registers (54284), 30% of the slice LUTs (46559) and 196% of the DSP48E1s (1508). Obviously, this is not implementable, because during the synthesis, the ISE software was forced to use DSP48E1s to implement the multipliers. In the actual hardware implementation, other parts of the logic resource can be allocated to do the multiplications. In this way, Scheme 1 used 16% of the slice registers (49557), 30% of the slice LUTs (46411) and 100% of the DSP48E1s (768), so all the DSP functions still fit into the XC6VLX240T. It is clear that Scheme 1 has saved around 30% of logic resources compared with Scheme 2. This represents a significant reduction of hardware, especially for the required number of multipliers, which usually dominate the computational complexity in the IFFT implementation. Our proposed Scheme 1 can not only help to save power but also make it easily implementable in a FPGA that has limited hardware resources. This is very important for optical communication systems, which have a very high data throughput, requiring the very fast FPGAs.

For standard L/EACO-OFDM, only the real outputs of the IFFTs are used, so all the computational units used to calculate the imaginary outputs of the IFFT's final butterfly can be eliminated. However, the single-IFFT ASE-DMT transmitter requires both the real and imaginary outputs of IFFT. Therefore, the single-IFFT ASE-DMT transmitter occupies approximately 30% more logic resources compared with a hardware-efficient L/EACO-OFDM transmitter [20]. A multiple-IFFT ASE-DMT transmitter would, however, require 85% more resources than this hardware-efficient L/EACO transmitter.

IV. EXPERIMENTAL SETUP

Fig. 4 (a) and (b) show the experimental setup. A 156.25-MHz clock generated by the DAC provided a clock for the FPGA, which was used to control all the DSP modules in the FPGA and synchronize the FPGA and DAC. The DAC and FPGA channels were connected via 20 pairs of coaxial cables for LVDS. The MICRAM DAC had a resolution of 6 bits, so full operation would require 24 high-speed transmitter channels from the FPGA. However, as there were only 20 high-speed transmitters available on our FPGA evaluation board (ML623), the four inputs corresponding to the least significant bit of DAC were connected to logic zero, which led to a 5-bit resolution. Because 118 data bits were encoded and 32-sample CP was appended in one clock, the net data rate was 18.4 Gb/s.

The DAC's analog output signal was around 500 mV peak-to-peak. The signal was attenuated by 18 dB, then fed through a 24-dB gain 40-GHz bandwidth linear electrical amplifier (SHF-807). The resulting 1-volt (p-p) output was connected to the 1550-nm distributed feedback laser biased at 36 mA. A variable optical attenuator (VOA) was used to adjust the output optical power, followed by a 16-GHz photodetector (DSC-40S) to convert optical signals to electrical signals, which were then sampled by a real-time Digital Storage Oscilloscope (DSO-X92804A) with an 80-GS/s sampling rate. Finally, the captured samples were analyzed by off-line DSP in MATLAB. The off-line DSP algorithm is illustrated in Fig. 4(c). After the frame synchronization, serial to parallel conversion and CP removal were conducted, followed by a one-tap equalizer before the iterative decoding process was performed to decode the data layer by layer. Some key parameters in the entire transmission link are summarized in Table I.

V. EXPERIMENTAL RESULTS

A. Electrical Back-to-Back

Firstly, the Q-factor performance for electrical back-to-back configuration (see Fig. 4(b)) was measured by connecting the DAC output directly to a DSO. The captured samples were analyzed by off-line DSP in MATLAB and the results are shown in Fig. 5. As the Q-factors of adjacent-index subcarriers for the different layers are very similar, we can conclude that

the iterative algorithm in the receiver substantially cancels the clipping distortion, without error propagation.

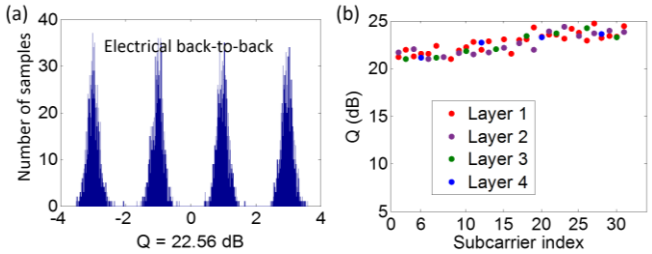

Fig. 5. Histogram of amplitudes (a) and Q-factor *vs* subcarrier index (b) for electrical back-to-back. The four slicing points for PAM4 in (a) is -3, -1, 1, and 3.

B. Optical Back-to-Back

The optical back-to-back Q-factor was measured by directly connecting the laser output to the VOA. With zero optical attenuation, the optical power received by the photodetector was 3.53 dBm. As shown in Fig. 6, the average Q-factor is 19.67 dB. There is a 3-dB penalty for the highest-frequency subcarriers, resulting from the limited laser bandwidth. The Q-factors for nearby frequencies are still similar. Additional signal quality degradation is not seen in the high layers, indicating that there is little error propagation.

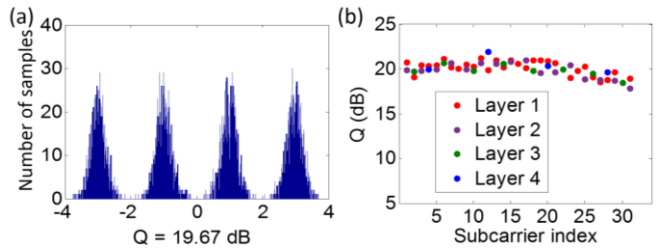

Fig. 6. Histograms of amplitudes (a) and Q-factor *vs* subcarrier index (b) for optical back-to-back. The four slicing points for PAM4 in (a) is -3, -1, 1, and 3.

C. Fiber Transmission

Finally, the bit-error-ratios (BER) and Q-factors for 10-km and 20-km SSMF transmission are shown in Fig. 7 and Fig. 8 separately. The optical power after transmission over 10-km SSMF was 0.4 dBm and the average Q-factor was 18.51 dB, as shown in Fig. 7. There is a 5-dB penalty for the highest-frequency subcarriers; a 2-dB increase compared with optical back-to-back. This is probably because of the uneven channel response induced by the interaction of laser chirp and fiber dispersion, which can be seen more clearly in Fig. 8. After 20-km SSMF transmission, the optical power reduced to -2.62 dBm and the signal qualities for higher-frequency subcarriers are seriously degraded. Even in the first layer, the Q-factors of the higher-frequency subcarriers are below 10 dB. A Q-factor of <10 dB means a very large number of decoding errors for PAM4. The iterative receiver will pass these decoding errors from the lower layers to the higher layers; that is why the lowest Q-factors are seen in the highest layer. Therefore, the BER after 20-km SSMF transmission is >0.1.

In order to identify the influence of fiber dispersion, the optical power attenuation was set to 6.15 dB (3.53 dBm – (-2.62 dBm)) by the VOA, to mimic the power attenuation of

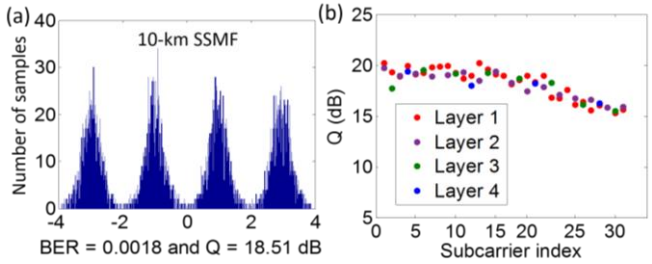

Fig. 7. Histograms of amplitudes (a) and Q-factor *vs* subcarrier index (b) after 10-km transmission. The four slicing points for PAM4 in (a) is -3, -1, 1, and 3.

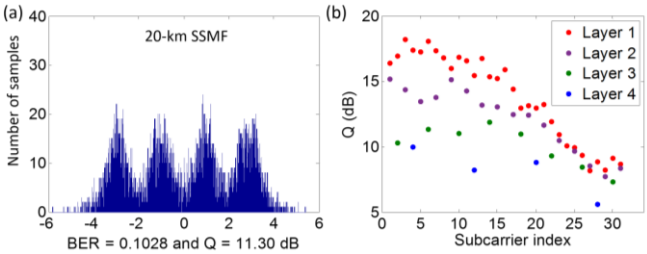

Fig. 8. Histograms of amplitudes (a) and Q-factor *vs* subcarrier index (b) after 20-km transmission. The four slicing points for PAM4 in (a) is -3, -1, 1, and 3.

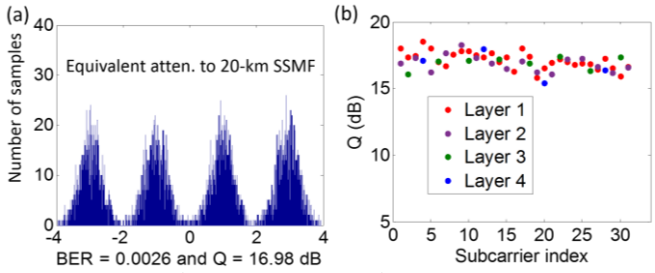

Fig. 9. Histograms of amplitudes (a) and Q-factor *vs* subcarrier index (b) after 6.15 dB power attenuation (equivalent attenuation of 20-km SSMF transmission). The four slicing points for PAM4 in (a) is -3, -1, 1, and 3.

the 20-km SSMF and optical connectors. With no fiber transmission, the Q-factor was measured and is shown in Fig. 9. The average Q-factor is around 17 dB and it is almost equal for the adjacent subcarriers in all the four layers; no decoding error propagation occurs between different layers. The BER is 2.6×10^{-3}, is still below the 7% FEC limit, corresponding to the BER of 3.8×10^{-3}. Both the Q-factors and BERs shown in Fig. 9 are significantly better when compared with those in Fig. 8, which means that the 6.15-dB power attenuation from the 20-km SSMF and optical connectors cannot alone lead to the transmission failure. Therefore, we can conclude that the serious higher-frequency signal quality degradation, as shown in Fig. 8, leads to the transmission failure over 20-km SSMF, which mainly result from the interaction of laser chirp and fiber dispersion.

VI. Conclusions

In this paper, a computationally efficient real-time PAM4 modulated ASE-DMT transmitter, with a net data rate of 18.4 Gb/s, has been proposed and experimentally demonstrated. ASE-DMT usually requires one IFFT per layer, we show that by inputs mapping and extracting outputs from within the IFFT, only one IFFT is required to generate the outputs of all the layers. By implementing within one FPGA chip, 30% logic

resource utilization can be saved, compared with a common ASE-DMT transmitter using one IFFT per layer. The same method can also be used in other layered schemes such as L/EACO-OFDM; this will be demonstrated in our future work. With off-line signal processing in the receiver, the ASE-DMT signals have been successfully transmitted over 10-km SSMF. More than 20-km SSMF transmission could be achieved by using a higher resolution DAC, pairwise coding [24], only using a single sideband to reduce the influence of chromatic dispersion [5], or by using bit- and power-loading [9].

REFERENCES

[1] A. J. Lowery, and L. B. Du, "Optical orthogonal division multiplexing for long haul optical communications: A review of the first five years," Optical Fiber Technology, vol. 17, no. 5, pp. 421-438, 2011.

[2] B. J.C. Schmidt, A. J. Lowery, and J. Armstrong, "Experimental demonstrations of electronic dispersion compensation for long-haul transmission using direct-detection optical OFDM," J. Lightw. Technol., vol. 26, no. 1, pp. 196-203, 2008.

[3] N. Cvijetic, "OFDM for next-generation optical access networks," J. Lightw. Technol., vol. 30, no. 4, pp. 384-398, 2012.

[4] J. Wei, Q. Cheng, R. V. Penty, I. H. White, and D. G. Cunningham, "400 Gigabit Ethernet using advanced modulation formats: performance, complexity, and power dissipation," IEEE Communications Magazine, vol. 53, no. 2, pp. 182-189, 2015.

[5] L. Zhang, T. Zuo, Y. Mao, Q. Zhang, E. Zhou, G. Ning Liu, and X. Xu, "Beyond 100-Gb/s transmission over 80-km SMF using direct-detection SSB-DMT at C-band," J. Lightw. Technol., vol. 34, no. 2, pp. 723-729 2016.

[6] Z. Liu, B. Kelly, J. O'Carroll, R. Phelan, D. J. Richardson, and R. Slavík, "Discrete multitone format for repeater-less direct-modulation direct-detection over 150 km," J. Lightw. Technol., vol. 34, no. 13, pp. 3223-3229, 2016.

[7] A. Dochhan, H. Griesser, N. Eiselt, M. H. Eiselt, and J. Elbers, "Solutions for 80 km DWDM systems," J. Lightw. Technol., vol. 34, no. 2, pp. 491-499, 2016.

[8] Y. Benlachtar *et al*., "Generation of optical OFDM signals using 21.4 GS/s real time digital signal processing," Opt. Express, vol. 17, no. 20, pp. 17658-17668, 2009.

[9] R. P. Giddings *et al*., "Experimental demonstration of a record high 11.25 Gb/s real-time optical OFDM transceiver supporting 25km SMF end-to-end transmission in simple IMDD systems," Opt. Express, vol. 18, no. 6, pp. 5541-5555, 2010.

[10] M. Chen, J. He, and L. Chen, "Real-time demonstration of 1024-QAM OFDM transmitter in short-reach IMDD systems," IEEE Photonics Technol. Lett. vol. 27, no. 8, pp. 824-827, 2015.

[11] J. Armstrong and A. J. Lowery, "Power efficient optical OFDM," Electron. Lett., vol 42, no. 6, pp. 370-372, 2006.

[12] S. C. J. Lee, S. Randel, F. Breyer, and A. M. Koonen, "PAM-DMT for intensity-modulated and direct-detection optical communication systems," IEEE Photon. Technol. Lett., vol. 21, no. 23, pp. 1749-1751, 2009.

[13] J. K. Perin, M. Sharif, and J. M. Kahn, "Modulation schemes for single-laser 100 Gb/s links: multicarrier," J. Lightw. Technol., vol. 33, no. 24, pp. 5122-5132, 2015.

[14] L. Chen, B. Krongold, and J. Evans, "Successive decoding of anti-periodic OFDM signals in IM/DD optical channel," in *Proceedings of IEEE International Conference on Communications*, Cape Town, South Africa, PP. 1-6, 2010.

[15] Q. Wang, C. Qian, X. Guo, Z. Wang, D. G. Cunningham, and I. H. White, "Layered ACO-OFDM for intensity-modulated direct-detection optical wireless transmission," Opt. Exp., vol. 23, no. 9, pp. 12382-12393, 2015.

[16] A. J. Lowery, "Comparisons of spectrally-enhanced asymmetrically-clipped optical OFDM systems," Opt. Exp., vol. 24, no. 4, pp. 3950-3966, 2016.

[17] M. S. Islim, D. Tsonev, and H. Haas, "On the superposition modulation for OFDM-based optical wireless communication," in *Proceedings of IEEE Global Conference on Signal and Information Processing*, Orlando, American, pp. 1022-1026, 2015.

[18] B. Song, C. Zhu, B. Corcoran, Q. Wang, L. Zhuang, and A. J. Lowery, "Experimental layered/enhanced ACO-OFDM short-haul optical fiber link," IEEE Photonics Technol. Lett., vol. 28, no. 24, pp. 2815-2818, 2016.

[19] M. S. Islim, and H. Haas, "Augmenting the spectral efficiency of enhanced PAM-DMT-based optical wireless communications," Opt. Exp., Vol. 24, no. 11, pp. 11932-11949, 2016.

[20] Q. Wang, B. Song, B. Corcoran, D. Boland, C. Zhu, L. Zhuang, and A. J. Lowery, "Hardware-efficient signal generation of layered/enhanced ACO-OFDM for short-haul fiber-optic links," Opt. Express, vol. 25, no. 12, pp. 13359-13371, 2017.

[21] Q. Wang, B. Song, B. Corcoran, L. Zhuang, A. Lowery, "Single IFFT augmented spectral efficiency DMT transmitter," accepted by ECOC 2017, Gothenburg, Sweden.

[22] H. Sorensen, D. Jones, M. Heideman, and C. Burrus, "Real-valued fast Fourier transform algorithms," IEEE Trans. Acoustics, Speech, and Signal Proc., vol. 35, no. 6, pp. 849-863, 1987.

[23] P. A. Milder, F. Franchetti, J. C. Hoe, and M. Püschel, "Computer generation of hardware for linear digital signal processing transforms," ACM Trans. on Design Automation of Electronic Systems, vol. 17, no. 2, pp. 15, 2012.

[24] B. Song, B. Corcoran, Q. Wang, L. Zhuang, and A. J. Lowery, "Subcarrier pairwise coding for short-haul L/E-ACO-OFDM," IEEE Photonics Technol. Lett., vol. 29, no. 18, pp. 1584-1587, 2017.